

Periodicity search for Pulsar Binaries with *TESS*

PARTHA SARATHI PAL,¹ P. H. T. TAM,¹ WEITANG LIANG,¹ CHENGYE CAO,¹ K. L. LI,² C. Y. HUI,³ AND A. K. H. KONG²

¹*School of Physics and Astronomy, Sun Yat Sen University, Guangzhou 510275, China*

²*Institute of Astronomy, National Tsing Hua University, Hsinchu 30013, Taiwan*

³*Department of Astronomy & Space Science, Chungnam National University, Daejeon 34134, Korea*

ABSTRACT

Pulsar binaries, in particular redback systems, provide good sources to study the pulsar wind flow and its interaction with the companion stars. *Fermi*-LAT have proposed probable pulsar binary candidates in its catalogs. To identify pulsar binary sources from the catalog, orbital modulation search of binary candidates is an effective way. *TESS* observes in survey mode for a large part of the sky and thus provide an excellent data set to periodicity search of pulsar binary candidates by observing the flux variation, thought to mainly come from the stellar companion. Using *TESS* data we look for flux modulation of five pulsar binaries (or candidates) with reported orbital periods, including PSR J1023+0038, 3FGL J0523.3-2528, 3FGL J0212.1+5320, 3FGL J0744.1-2523 and PSR J1417-4402, demonstrating that *TESS* photometric data are very useful in identifying periodicities of redback-like systems. This method can be effective in searches for new pulsar binaries or similar binary systems in the future.

Keywords: methods: data analysis — pulsars: general — X-rays: binaries — (stars:) pulsars: individual (PSR J1023+0038, 3FGL J0523.3-2528, 3FGL J0212.1+5320, 3FGL J0744.1-2523, PSR J1417-4402)

1. INTRODUCTION

Redback systems are close-orbit pulsar binaries that show intense interactions between the pulsars and the companion stars. The orbital period of redbacks typically spans $P_b \leq 20$ hrs (Roberts 2013; Hui & Li 2019), with an exception PSR J1306-40 $P_b = 26.3$ hrs (Linares 2018; Swihart et al. 2019). The companion stars are late-type non-degenerate ones with masses of $M_c \sim 0.2 - 0.5 M_\odot$, which are significantly higher than those of another similar class of systems, black widows, for which $M_c < 0.1 M_\odot$ (Roberts 2013; Hui & Li 2019). Some redbacks have been observed to transit between the rotational-powered state and a state with an accretion disk, such as those observed in PSR J1023+0038 and XSS J12270-4859 (see, e.g. Archibald et al. 2009; Papitto et al. 2013; Patruno et al. 2014; Stappers et al. 2014; Bassa et al. 2014; Takata et al. 2014; Roy et al. 2015, and references therein). Pulsar binaries of longer

orbital periods than one day, such as PSR J1417-4402, have also been discovered (e.g. Swihart et al. 2018).

Optical periodicity related to the pulsar irradiation and ellipsoidal variation have been observed in many of the known pulsar binaries. At the same time, non-periodic phenomena such as optical flares (e.g., from the accretion disk) and flux change (between different states/modes) at various time scales can also be used to probe the astrophysical conditions of the systems.

Transiting Exoplanet Survey Satellite (TESS) is a survey satellite with a bandpass of 600 – 1000 nm whose principal mission is to observe flux variation of stars to determine the presence of exoplanets around those stars (Ricker et al. 2015). With its supreme timing ability at time scales of minutes to hours and its nearly all-sky coverage, it is also an ideal instrument to characterize periodicities and flux variations of stars (Dorn-Wallenstein et al. 2019; Balona & Ozuyar 2020) and binaries, such as redbacks either in their accretion or rotation-powered states.

In this work, we searched through the literature for known redback-like pulsar binaries (or candidates) with reported orbital period, including those covered by *TESS* target products. The chosen sources are given

Corresponding author: P. H. T. Tam
tanbxuan@mail.sysu.edu.cn

in Table. 1. The aim is to demonstrate the photometric capabilities of *TESS* to characterize redbacks and similar systems.

2. THE REDBACK SYSTEMS (CANDIDATES)

2.1. PSR J1023+0038

The prototypical redback pulsar, PSR J1023+0038, has shown transitions between a LMXB state and a rotational-powered state (see, e.g., Archibald et al. 2009; Tam et al. 2010; Patruno et al. 2014; Stappers et al. 2014). A single-humped modulation in optical for 4.75 hr was first reported in Woudt et al. (2004), during the time now believed to be a pulsar state. Time-resolved optical spectroscopy and photometry of PSR J1023+0038 revealed that it is an X-ray binary and consists of a late type G5 companion star with a period of 4.75 hr (Thorstensen & Armstrong 2005). Subsequently, detection of a pulsar spin period of 1.69 ms in 2007 confirmed the primary as a radio millisecond pulsar (Archibald et al. 2009). Using further observations, it has been found that the donor star has a mass $M_2 \sim 0.24M_\odot$, $M_{NS} = 1.71 \pm 0.16M_\odot$, and the binary at a distance $d = 1.37 \pm 0.04$ kpc (Deller et al. 2012; McConnell et al. 2015). In 2013 the transition from MSP to LMXB state of PSR J1023+0038 was reported with disappearance of radio pulsation and increase in optical, X-ray and γ -ray fluxes (Patruno et al. 2014; Stappers et al. 2014; Takata et al. 2014).

Since then, in the current accretion state, PSR J1023+0038 shows rapid flickering and double-peaked emission lines in a blue optical spectrum, believed to be associated with an accretion disc (e.g. Kennedy et al. 2018; Shahbaz et al. 2019), as first seen in the previous accretion state (Szkody et al. 2003).

On 2019-02-02 20:09:35 UTC *TESS* has observed PSR J1023+0038 for 27 days under *TESS* GI Proposal id: #G011187 (PI: Mark Kennedy).

2.2. 3FGL J0523.3-2528

1FGL J0523.5-2529 was discovered as a *Fermi-LAT* unidentified γ -ray source (Abdo et al. 2010), without detected radio emission yet (Guillemot et al. 2012; Petrov et al. 2013). Later it was recataloged as 3FGL J0523.3-2528 (Acero et al. 2015). The optical photometry and *SOAR* spectroscopic observations of a X-ray source detected within the localization error of 3FGL J0523.3-2528 revealed a periodic flux modulation of 16.5 hr period (Strader et al. 2014). The radial velocity variations indicate a probable binary pulsar with an unusually massive ($0.8 M_\odot$) secondary companion and a measurable eccentricity ($e = 0.04$) (Strader et al. 2014).

On 2018-11-15 11:25:39 UTC, 2018-12-15 18:27:39 UTC; *TESS* has observed 3FGL J0523.3-2528 for 54 days under *TESS* GI Proposal id: #G011187 (PI: Mark Kennedy).

2.3. 3FGL J0212.1+5320

3FGL J0212.1+5320 was first discovered as an unidentified γ -ray source, 1FGL J0212.3 + 5319 (Abdo et al. 2010). Detailed photometry and optical spectroscopy classified 3FGL J0212.1+5320 as a redback MSP candidate with a period of 0.87 days (Li et al. 2016; Linares et al. 2017). From spectroscopic modeling of 3FGL J0212.1+5320 optical data, it is reported that 3FGL J0212.1+5320 binary system may consists of a neutron star and secondary star mass of $M_1 = 1.85_{-0.26}^{+0.32}M_\odot$ and $M_2 = 0.50_{-0.19}^{+0.22}M_\odot$ respectively (Shahbaz et al. 2017).

On 2019-11-03 03:35:25 UTC, *TESS* has observed 3FGL J0212.1+5320 for 27 days exposure time under *TESS* GI Proposal id: #G022055 (PI: Francesco Coti Zelati).

2.4. 3FGL J0744.1-2523

3FGL J0744.1-2523 was detected as an unidentified γ -ray source. No associated X-ray source, within 0.3-10 keV $3\text{-}\sigma$ upper limit, is detected down to a limit of 4.5×10^{-14} ergs $s^{-1} cm^{-2}$. The field of 3FGL J0744.1-2523 is not covered by the Catalina Sky Survey. A variable *GROND* source within the error ellipse of 3FGL J0744.1-2523 has been found. This source features a clear flux modulation with an optical and near-IR period equal to 0.115 day (Salvetti et al. 2017). We note that such a candidate optical counterpart is now outside the 4FGL error circle, and no bright radio or optical counterpart can be found within the 4FGL 95% error circle.

On 2019-01-08 02:59:36 UTC, *TESS* has observed 3FGL J0744.1-2523 sky location during Sector: #7 of its survey mode for 27 days exposure time.

2.5. PSR J1417-4402

PSR J1417-4402 was detected as a γ -ray source by *Fermi-LAT* and cataloged as 3FGL J1417.5-4402 (Abdo et al. 2010). Photometric and spectroscopic analysis of the optical counterpart reported a period of 5.37 day, with no significant eccentricity, at a distance of 4.4 kpc. The mass ratio of the system is predicted around $\frac{M_2}{M_{NS}} = 0.18$. The estimated mass of the components are $M_{NS} = 1.97 \pm 0.15M_\odot$ and $M_2 = 0.35 \pm 0.04M_\odot$ (Strader et al. 2015). A 2.66 ms radio pulsar PSR J1417-4402 has been found and the distance from radio data is estimated to be 1.6 kpc (Camilo et al. 2016). Subsequently, PSR J1417-4402

Table 1. List of sources analysed: (1) Source names, (2) Right Accession, (3) Declination, (4) Observation start time, (5) Observation stop time, (6) Sector, (7) Camera No., (8) CCD No., (9) *TESS* magnitude.

Source Name	RA	Dec	Start time	Stop time	Sector	Camera	CCD	<i>TESS</i>
	(°)	(°)	(UTC)	(UTC)	(#)	(#)	(#)	(Mag.)
(1)	(2)	(3)	(4)	(5)	(6)	(7)	(8)	(9)
PSR J1023+0038	155.948668	0.644794	2019-02-02 20:09:36	2019-02-27 11:59:35	8	1	3	16.28
3FGL J0523.3-2528	80.820517	-25.460263	2018-11-15 11:25:40	2018-12-11 18:53:39	5	2	2	15.78
			2018-12-15 18:27:39	2019-01-06 13:03:39	6	2	1	15.78
3FGL J0212.1+5320	33.043655	53.360771	2019-11-03 03:35:26	2019-11-27 12:43:25	18	2	3	13.85
3FGL J0744.1-2523	116.044700	-25.399400	2019-01-08 02:59:37	2019-02-01 13:59:36	7	2	2	...
PSR J1417-4402	214.377517	-44.049269	2019-04-23 06:29:33	2019-05-20 08:59:32	11	1	2	...

is classified to be a redback-like system (Swihart et al. 2018; De Vito et al. 2019).

On 2019-04-23 06:29:33 UTC, *TESS* has observed PSR J1417-4402 sky location during Sector: #11 of its survey mode for 27 days exposure time.

3. DATA ANALYSIS

Periodicity searches were performed using archival *TESS* data. The obtained periodicity is then compared to the reported orbital periods.

The *TESS* archival data are searched and obtained with *Astroquery*. PSR J1023+0038, 3FGL J0523.3-2528, 3FGL J0212.1+5320 are observed under *TESS* Guest Investigator Program. For these three sources 2 min cadence `timeseries` data are downloaded. For 3FGL J0744.1-2523 and PSR J1417-4402, *TESSCUT* 30 min cadence FFI data within $3.85' \times 3.85'$ are downloaded. All data are analysed with *Lightkurve* (Lightkurve Collaboration et al. 2018). Light curve files are generated with `to_lightcurve()` from calibrated target-pixel files. For GI proposal data *lightkurve*-defined aperture mask `pipeline_mask` for GI proposal data. For 3FGL J0744.1-2523 *TESSCUT* data aperture mask is chosen manually depending upon the presence of peak profile in PDSs of the individual pixels. The infinite or NaN values are excluded from light curves with `remove_nans()`. The outliers above $3\text{-}\sigma$ level in the light curves are clipped with `remove_outliers()`. The threshold for PSR J1023+0038 is set to $6\text{-}\sigma$ to retain the flaring events. All cleaned unbinned light curves are plotted in the top panel of Fig. 2(a-d). In order to search periodicities in the optical flux Power Density Spectra are generated with `to_periodogram` from cleaned unbinned light curves. Power Density Spectra are calculated using *Lomb-Scargle* method and normalized to power spectral density (Balona & Ozuyar 2020).

Significant peak profiles in power density spectra are determined with *Bayesian block* analysis (Scargle et al. 2013) with 95% statistical significance using *Astropy*. The peak profiles obtained from *Bayesian block* analysis are fitted with a *Lorentzian* profile (Belloni et al. 2002) using *Scipy* to estimate the significance of the peak profiles. From curve fitting Q-value ($\frac{\nu}{\Delta\nu}$) (Casella et al. 2005), RMS amplitude¹ [see Eq. 1] and reduced χ^2 are calculated as goodness of fit. The $1\text{-}\sigma$ error bars are estimated from covariance matrix. The analysis results are shown in Table 2. In middle panel of Fig. 2(a-d) PDSs are shown in black color. The *Bayesian* blocks are shown in grey dashed lines. The *Lorentzian* peak profiles are shown in red, green, blue dashed lines. The continuum part of the PDS is fitted with power-law model and shown in magenta dashed line as an estimation of noise in the PDS.

$$RMS = 100 \times \sqrt{\frac{A}{Flux}}\%, \quad (1)$$

$$\text{where, } A = \frac{\pi}{2} \times \text{Normalization} \times FWHM,$$

$$= \text{Flux under Lorentzian function};$$

$$\text{Normalization} = \text{Power at peak frequency},$$

$$FWHM = \text{Full width half maxima}.$$

Before detailed analysis for individual sources, one would like to first verify that the obtained periodicity in the PDS indeed comes from the corresponding redback positions. Hence, PDSs of pixels around aperture mask (i.e., neighborhood pixels) are plotted with *Bayesian* blocks, as shown in Fig. 1(a-d). In Fig. 1(a-c) the blue boxes mark the pixels included in the pipeline-defined aperture mask. For 3FGL J0744.1-2523 in Fig. 1(d),

¹ https://heasarc.gsfc.nasa.gov/docs/xte/recipes/pca_fourier.html

the 5×5 pixel PDS plot with peak profiles at the same frequencies are observed. The pixel with the strongest peak profile is taken as aperture mask for the further analysis of 3FGL J0744.1-2523 *TESS* data (marked with a red box). For PSR J1417-4402 in Fig. 3(a), the 5×5 pixel PDS plot is shown where no peak profile is observed. The pixel coordinates are projected on sky coordinates and PSR J1417-4402 sky coordinates coincides with pixel #13, which is marked with a blue box. This pixel is taken as aperture mask for further analysis of PSR J1417-4402 *TESS* data.

With the obtained orbit-related periodicities of red-back systems (candidates) using *TESS* data, we then fold the *TESS* light curves for four sources with the orbital period, as shown in bottom panel of Fig. 2(a-d) and Fig. 3(b). The low frequency trends are removed from data using *Savitzky-Golay* filter. The flux is normalized to the median flux of each source. The phase zero (T_0) is set to the inferior conjunction (when the companion is between the pulsar and the observer), following [Thorstensen & Armstrong \(2005\)](#) for PSR J1023+0038, [Linares et al. \(2017\)](#) for 3FGL J0212.1+5320, [Strader et al. \(2014\)](#) for 3FGL J0523.3-2528 and [Salvetti et al. \(2017\)](#) for 3FGL J0744.1-2523.

4. RESULTS

4.1. PSR J1023+0038

In *TESS* data PSR J1023+0038 shows a median flux around $60 e^- s^{-1}$ for around 26 days. The *Lomb-Scargle* periodogram and its *Bayesian* analysis shows a peak between 50-60 μHz with power around $10 \frac{e^-}{\mu\text{Hzs}^2}$ (see Fig. 2(a)). From these peak profile parameters a period of 4.7816 ± 0.0015 hr (i.e., corresponding to the reported orbital period) is obtained. The Q-value for this peak profile is 174.57 with 19.22% of flux photons responsible for the orbital modulation. The goodness of fit is 2.17(40). No other signature of periodicity is observed in the PDS. The continuum part before and after the orbital period is fitted with power-law models. The power-law index of lower-frequency part is $\Gamma_1 = 0.65 \pm 0.14$ and upper-frequency part is $\Gamma_2 = 1.2 \pm 0.05$.

Short-time flares are also seen, and are occurring as often as that reported in [Kennedy et al. \(2018\)](#); [Papitto et al. \(2019\)](#).

4.2. 3FGL J0523.3-2528

Fig. 2(b) shows the light curve of 3FGL J0523.3-2528. *TESS* has observed 3FGL J0523.3-2528 for a total of 50 days in two consecutive observation sectors (#5 and #6). We checked the full-frame images, finding that different pipeline-defined aperture masks are used dur-

ing two sectors. To maintain consistency, we here use the aperture mask defined by the pipeline for sector #5 for both sectors. The *Lomb-Scargle* periodogram and its *Bayesian* analysis shows 3 peak profiles. The fundamental frequency, shown in red dashed line, is observed at 33.56 μHz which represents a period of 8.28 hr with Q-value of 400.62 and 8.99% of observed flux photons responsible for the orbital motion. Around 16.89 μHz , blue dashed line, half-harmonic is observed which yields an oscillation of 16.44 hr with Q-value 165.42 and 2.68% observed flux involved in it. The goodness of fit is 0.12(19). The first harmonic of this orbital motion is also observed in the PDS at 67.26 μHz . This peak is less than 95% statistical significant. This peak is ignored. Another peak profile is observed at 50.48 μHz shown in green dashed line. This peak profile represent another orbital motion for 5.5 hr with 219.18 Q-value and 3.02% RMS amplitude. The continuum at lower frequency shows power-law index of $\Gamma_1 = 0.02 \pm 0.9$ and upper-frequency shows $\Gamma_2 = 0.21 \pm 0.03$.

TESS data reveal the orbital period (16.5 hr, [Strader et al. 2014](#)) and also a period of 8.27 hr (one half of the orbital period) which is characteristic of ellipsoidal variation (EV). In the *TESS* PDS another periodicity of 5.5 hr is obtained with significant Q-value and RMS. This periodicity may represent some periodicity in the 3FGL J0523.3-2528 system which has not been reported before. Around 4.14 hr (i.e. 67 μHz) another peak may be seen which is likely a harmonic of the EV frequency. This peak profile is below 95% *Bayesian* block significance.

4.3. 3FGL J0212.1+5320

Fig. 2(c) shows the light curve of 3FGL J0212.1+5320. This light curve is affected by background scattering² and so we select those part of the data without severe scattering. Between TJD 1790-1795 a flare up to 300 $e^- s^{-1}$ is observed, after that the flux increases gradually. We believe such an increase is genuine as we also observe changes in the phase profile as the brightness changes (but not during the ‘steady flux’ state seen after TJD 1803). *Bayesian* block analysis of the PDS shows a peak profile around 26.53 μHz . This represents a period of 10.47 hr with 625.48 Q-value and 15.74% flux contribution for the orbital motion. The continuum at upper-frequency shows power-law index of $\Gamma = 2.34 \pm 0.10$.

This value is about twice that of the orbital period of 0.87 days, or 20.88 hr ([Li et al. 2016](#); [Linares et al. 2017](#)). In the *TESS* PDS pulse profile, no peak is located

² https://archive.stsci.edu/missions/tess/doc/tess_drn/tess_sector_18_drn25_

Table 2. PDS fitting results: (1) Source names, (2) Orbital period calculated from the peak frequency of *Lorentzian* profile, (3) Full Width Half Maximum of *Lorentzian*, (4) Q-value, (5) RMS amplitude (%), (6) Reduced χ^2 value.

Source Name	Period	FWHM	Q-value	RMS	χ^2_ν
	(hr)	(hr)		(%)	(dof)
(1)	(2)	(3)	(4)	(5)	(6)
PSR J1023+0038	4.7816 ± 0.0015	0.0274 ± 0.0027	174.57	19.22	2.17(40)
	8.2768 ± 0.0020	0.0207 ± 0.0010	400.62	8.99	0.65(55)
3FGL J0523.3-2528	16.4411 ± 0.0149	0.0994 ± 0.0068	165.42	2.68	0.12(19)
	5.5028 ± 0.0037	0.0251 ± 0.0041	219.18	3.02	0.07(42)
3FGL J0212.1+5320	10.4659 ± 0.0051	0.0167 ± 0.0751	625.48	15.74	0.08(18)
3FGL J0744.1-2523	2.7634 ± 0.0008	0.0034 ± 0.0015	815.86	0.70	0.01(38)

around 20.88 hr/13.3 μ Hz. However, a break in frequency domain is observed around this frequency which may cover a possible periodicity here.

4.4. 3FGL J0744.1-2523

In Fig. 2(d) the analysis result of 3FGL J0744.1-2523 Sector. #7 TESSCUT data is shown. The flux rate is within 190 $e^- s^{-1}$ and 195 $e^- s^{-1}$ for this observation. No strong flares are observed. Here in the PDS a pulse profile is observed from *Bayesian* block analysis. At 100.52 μ Hz one peak profile, is observed, shown in red color. This peak represents 2.76 hr period with Q-value = 815.86 and RMS = 0.7%. The flat continuum of PDS shows a power-law index of $\Gamma = 0.15 \pm 0.14$.

4.5. PSR J1417-4402

In Fig. 3(a) pixel-wise PDS diagram for PSR J1417-4402 is shown where no significant periodicity can be seen. The pixel #13 is analysed and shown in Fig. 3(b). We folded the light curve with the reported orbital period 5.37372(3) day (Camilo et al. 2016), corresponding to a frequency 2.15 μ Hz, as shown in Fig. 3(c). The uneven binning in the folded lightcurve is due to the time gap in the light curve.

5. DISCUSSION

The orbital period PSR J1023+0038 obtained in this work is formally not the same as reported earlier. A caveat in this work is that we did not exclude the flares from the original light curve, and so the flaring signals may contaminate the periodic signal. Since this work is mainly to demonstrate the TESS capability to search for periodicities from a large sample of sources, we did not attempt to remove the flares, as has been done in Kennedy et al. (2018); Pappitto et al. (2019) for the K2 80-day light curve with 58.8 s cadence.

Two peaks resulting from the secondary star’s ellipsoidal modulation can be seen in the orbital phased light

curves of 3FGL J0523.3-2528 and 3FGL J0212.1+5320 (see, bottom panel of Fig. 2(b-c)). Other than the two maxima and minima consistent with previous observations (Linares et al. 2017; Li et al. 2016; Strader et al. 2014), we find asymmetries in both minima and maxima. It confirms the findings of Li et al. (2016) and Linares et al. (2017) for 3FGL J0212.1+5320 and the asymmetry is first discovered for 3FGL J0523.3-2528 (whereas in previously reported light curve no significant asymmetry can be seen between the two maxima due to lower photometric accuracy Strader et al. 2014). While the unequal minima might be partly explained by limb- and gravity-darkening effects, the unequal maxima distinguishes these two pulsar binaries from normal ellipsoidal variables. Various models based on additional light source have been proposed to explain this phenomenon, such as off-center heating from an intra-binary shock (Romani & Sanchez 2016) or star-spot activity (van Staden & Antoniadis 2016).

For 3FGL J0212.1+5320, one may compare the EV-derived orbital period seen in *TESS* data (20.9318 ± 0.0102 hrs) taken around the mean MJD 58802) with that reported earlier in Li et al. (2016) ($20.8698(1)$ hrs taken at a mean MJD 57357) and Linares et al. (2017) ($20.8692(36)$ hrs, taken at a mean MJD 57218), showing plausible hint of increasing orbital period over time, but caution must be taken to over-interpret such a possibility.

For 3FGL J0744.1-2523, an optical period of 2.7701 ± 0.0012 hours is reported in Salvetti et al. (2017). The periodicity value 2.76342 ± 0.00079 obtained from our analysis is comparable with the literature value.

In the case of PSR J1417-4402 there is a flux gap within the light curve. Here we focus on periodicity analysis. The orbital period of PSR J1417-4402 is reported to be around 5.37372(3) days (Camilo et al. 2016). The effective exposure of the data analysed is

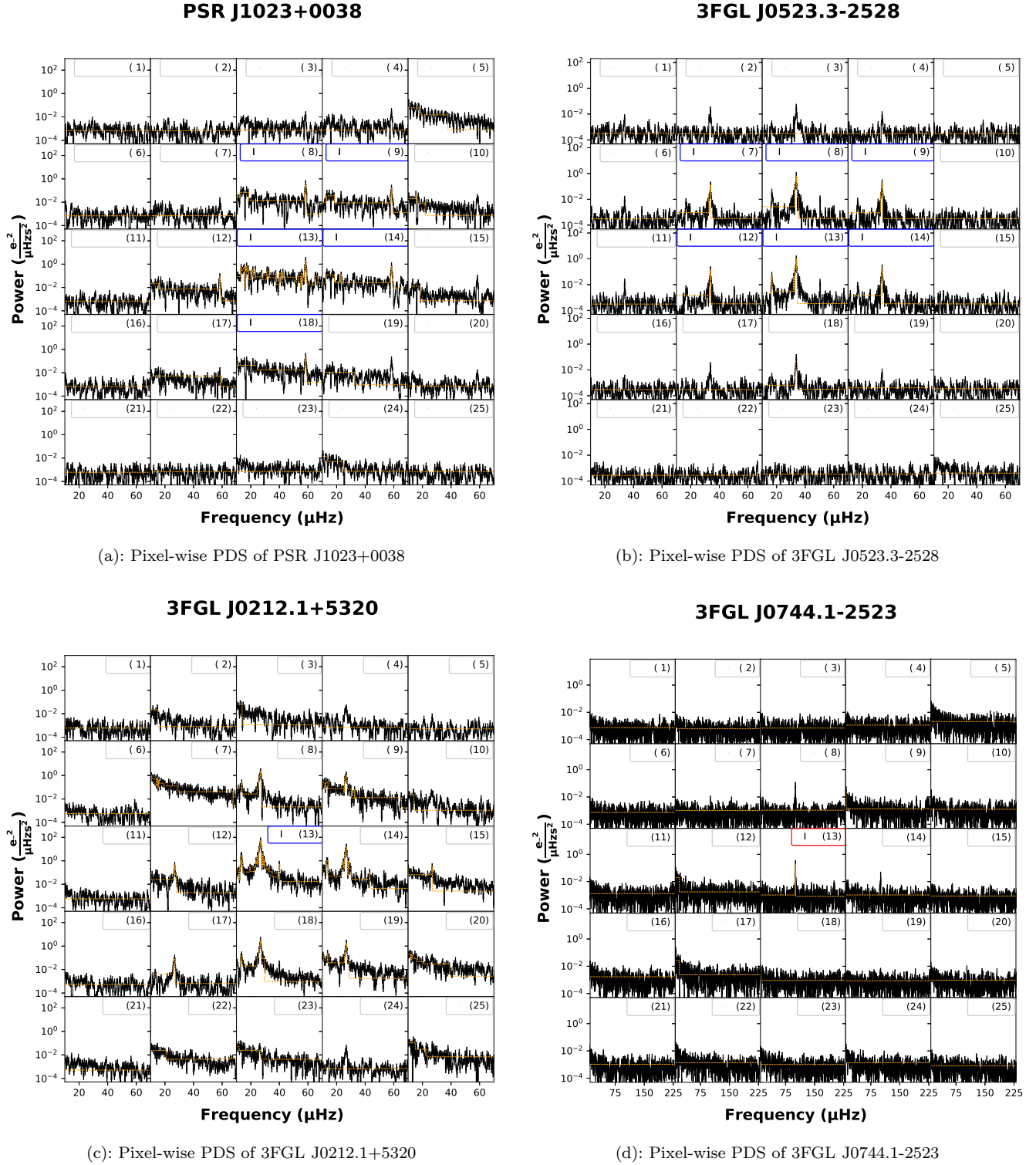


Figure 1. Pixel-wise power density spectra (black) along with Bayesian blocks (orange) from the pixels around the aperture mask. Blue boxes represent pipeline defined aperture mask. Red box represent manually chosen aperture mask with strongest peak profile.

around 10 days, a mere two orbital cycles. Combined with the flux gap and contamination from a nearby bright star, it may explain the non-detection of the period.

6. CONCLUSIONS

In this paper, *TESS* data from five pulsar binaries (or candidates thereof), are analysed. In two cases (i.e. PSR J1023+0038 and 3FGL J0744.1-2523) the period can be identified with the orbital period itself where the optical brightness variation may be due to pulsar irradiation. For other two cases (i.e. 3FGL J0523.3-2528, 3FGL J0212.1+5320), frequency peaks corresponding to literature values can be obtained and optical modulations are observed at half the orbital period values, which are EV signatures.

In summary, *TESS* data revealed periodicities seen in four previously reported redback-like systems. Analysis of *TESS* data for other similar binary systems will explore more information.

ACKNOWLEDGMENTS

PSP acknowledges SYSU-Postdoctoral Fellowship. PSP and PHT are supported by NSFC through grants 11633007, 11661161010 and U1731136. KLL is supported by the Ministry of Science and Technology (MOST) of the Republic of China (Taiwan) through grant 108-2112-M-007-025-MY3. CYH is supported by the National Research Foundation of Korea through grant 2016R1A5A1013277 and 2019R1F1A1062071. AKHK is supported by MOST of the Republic of China (Taiwan) through grant 105-2119-M-007-028-MY3. We thank Science Processing Operations Center (SPOC-NASA) and Mikulski Archive for Space Telescopes (MAST-STScI) for archival of the *TESS* data.

Facilities: *TESS*([Ricker et al. 2015](#))

Software: Astropy(v3.2.1 [Astropy Collaboration et al. 2013](#)), Astroquery([Ginsburg et al. 2013](#), v0.3.10), SciPy(v1.2.1 [Virtanen et al. 2019](#)), Lightkurve(v1.6 [Lightkurve Collaboration et al. 2018](#)), NumPy(v1.17.3 [van der Walt et al. 2011](#)).

REFERENCES

- Abdo, A. A., Ackermann, M., Ajello, M., et al. 2010, *ApJS*, 188, 405, doi: [10.1088/0067-0049/188/2/405](#)
- Acerro, F., Ackermann, M., Ajello, M., et al. 2015, *ApJS*, 218, 23, doi: [10.1088/0067-0049/218/2/23](#)
- Archibald, A. M., Stairs, I. H., Ransom, S. M., et al. 2009, *Science*, 324, 1411, doi: [10.1126/science.1172740](#)
- Astropy Collaboration, Robitaille, T. P., Tollerud, E. J., et al. 2013, *A&A*, 558, A33, doi: [10.1051/0004-6361/201322068](#)
- Balona, L. A., & Ozuyar, D. 2020, *MNRAS*, 493, 2528, doi: [10.1093/mnras/staa389](#)
- Bassa, C. G., Patruno, A., Hessels, J. W. T., et al. 2014, *MNRAS*, 441, 1825, doi: [10.1093/mnras/stu708](#)
- Belloni, T., Psaltis, D., & van der Klis, M. 2002, *ApJ*, 572, 392, doi: [10.1086/340290](#)
- Camilo, F., Reynolds, J. E., Ransom, S. M., et al. 2016, *ApJ*, 820, 6, doi: [10.3847/0004-637X/820/1/6](#)
- Casella, P., Belloni, T., & Stella, L. 2005, *ApJ*, 629, 403, doi: [10.1086/431174](#)
- De Vito, M. A., Horvath, J. E., & Benvenuto, O. G. 2019, *MNRAS*, 483, 4495, doi: [10.1093/mnras/sty3476](#)
- Deller, A. T., Archibald, A. M., Brisken, W. F., et al. 2012, *ApJL*, 756, L25, doi: [10.1088/2041-8205/756/2/L25](#)
- Dorn-Wallenstein, T. Z., Levesque, E. M., & Davenport, J. R. A. 2019, *ApJ*, 878, 155, doi: [10.3847/1538-4357/ab223f](#)
- Ginsburg, A., Robitaille, T., Parikh, M., et al. 2013, doi: [10.6084/m9.figshare.805208.v2](#)
- Guillemot, L., Freire, P. C. C., Cognard, I., et al. 2012, *MNRAS*, 422, 1294, doi: [10.1111/j.1365-2966.2012.20694.x](#)
- Hui, C. Y., & Li, K. L. 2019, *Galaxies*, 7, 93, doi: [10.3390/galaxies7040093](#)
- Kennedy, M. R., Clark, C. J., Voisin, G., & Breton, R. P. 2018, *MNRAS*, 477, 1120, doi: [10.1093/mnras/sty731](#)
- Li, K.-L., Kong, A. K. H., Hou, X., et al. 2016, *ApJ*, 833, 143, doi: [10.3847/1538-4357/833/2/143](#)
- Lightkurve Collaboration, Cardoso, J. V. d. M., Hedges, C., et al. 2018, Lightkurve: Kepler and TESS time series analysis in Python, Astrophysics Source Code Library. <http://ascl.net/1812.013>
- Linares, M. 2018, *MNRAS*, 473, L50, doi: [10.1093/mnrasl/slx153](#)
- Linares, M., Miles-Páez, P., Rodríguez-Gil, P., et al. 2017, *MNRAS*, 465, 4602, doi: [10.1093/mnras/stw3057](#)
- McConnell, O., Callanan, P. J., Kennedy, M., et al. 2015, *MNRAS*, 451, 3468, doi: [10.1093/mnras/stv1197](#)

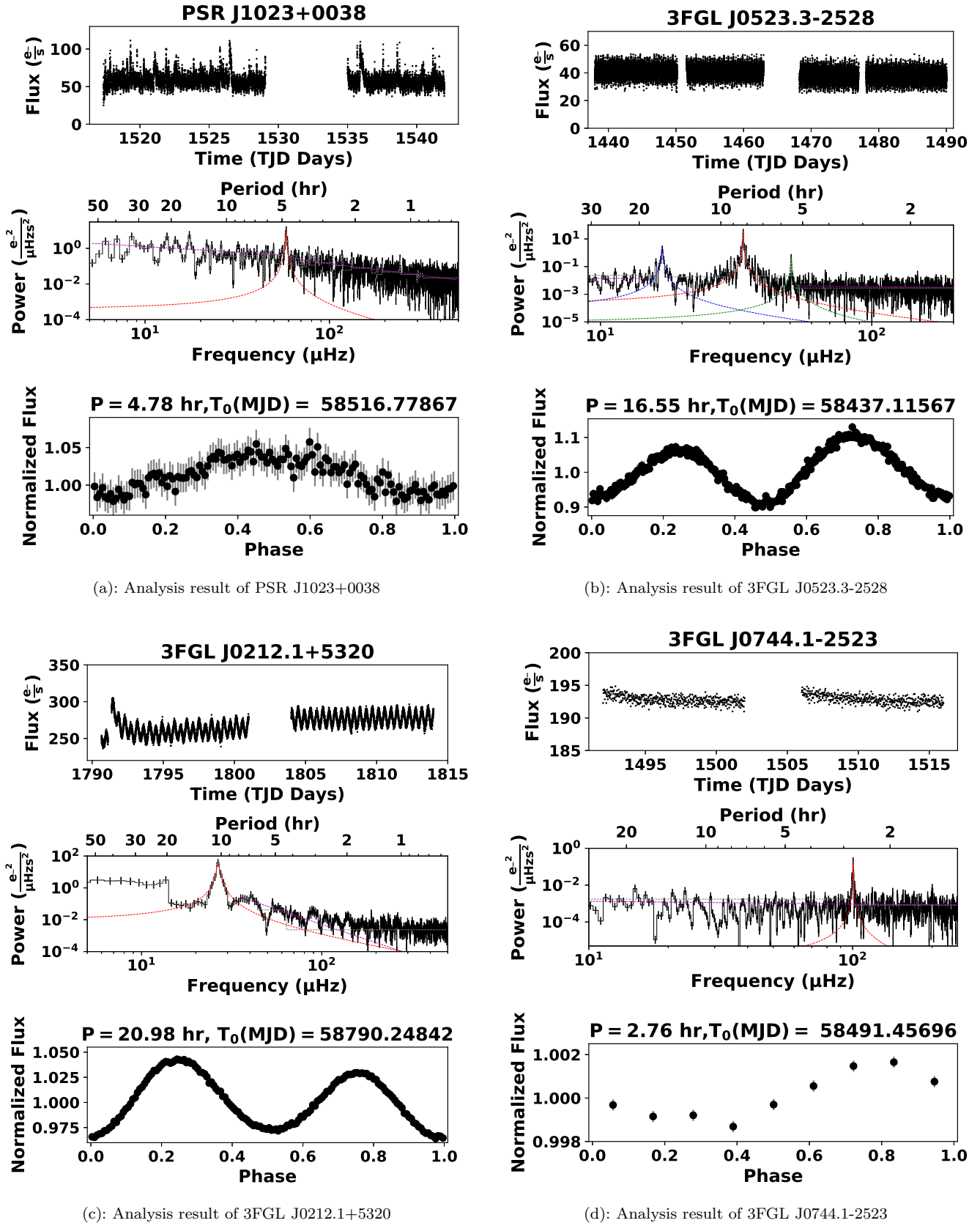


Figure 2. In all figures, top panel shows the unbinned *TESS* flux light curve; middle panel shows fitted PDS with *Bayesian* blocks and peak profiles; bottom panel shows the *TESS* light curves folded with periods shown above the panel.

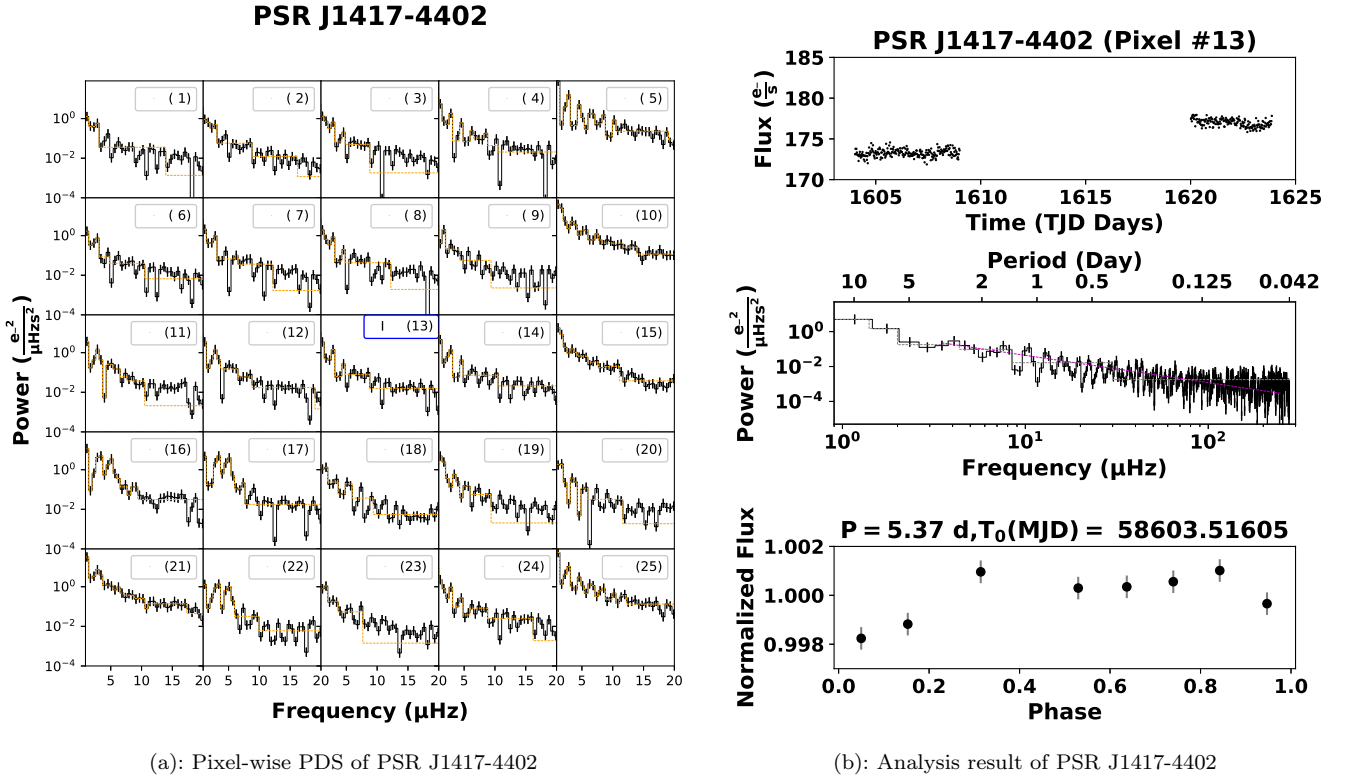


Figure 3. Pixel-wise Power Density Spectra (black) along with Bayesian blocks (orange), around the sky region of PSR J1417-4402. The sky location of PSR J1417-4402 superimposes on Pixel #13 (marked with blue). TESSCUT data from Pixel #13 are further analysed.

Papitto, A., Ferrigno, C., Bozzo, E., et al. 2013, *Nature*,

501, 517, doi: [10.1038/nature12470](https://doi.org/10.1038/nature12470)

Papitto, A., Ambrosino, F., Stella, L., et al. 2019, *ApJ*, 882,

104, doi: [10.3847/1538-4357/ab2fdf](https://doi.org/10.3847/1538-4357/ab2fdf)

Patruno, A., Archibald, A. M., Hessels, J. W. T., et al.

2014, *ApJL*, 781, L3, doi: [10.1088/2041-8205/781/1/L3](https://doi.org/10.1088/2041-8205/781/1/L3)

Petrov, L., Mahony, E. K., Edwards, P. G., et al. 2013,

MNRAS, 432, 1294, doi: [10.1093/mnras/stt550](https://doi.org/10.1093/mnras/stt550)

Ricker, G. R., Winn, J. N., Vanderspek, R., et al. 2015,

Journal of Astronomical Telescopes, Instruments, and Systems, 1, 014003, doi: [10.1117/1.JATIS.1.1.014003](https://doi.org/10.1117/1.JATIS.1.1.014003)

Roberts, M. S. E. 2013, in *IAU Symposium*, Vol. 291,

Neutron Stars and Pulsars: Challenges and Opportunities after 80 years, ed. J. van Leeuwen, 127–132, doi: [10.1017/S174392131202337X](https://doi.org/10.1017/S174392131202337X)

Romani, R. W., & Sanchez, N. 2016, *ApJ*, 828, 7,

doi: [10.3847/0004-637X/828/1/7](https://doi.org/10.3847/0004-637X/828/1/7)

Roy, J., Ray, P. S., Bhattacharyya, B., et al. 2015, *ApJL*,

800, L12, doi: [10.1088/2041-8205/800/1/L12](https://doi.org/10.1088/2041-8205/800/1/L12)

Salvetti, D., Mignani, R. P., De Luca, A., et al. 2017,

MNRAS, 470, 466, doi: [10.1093/mnras/stx1247](https://doi.org/10.1093/mnras/stx1247)

Scargle, J. D., Norris, J. P., Jackson, B., & Chiang, J. 2013,

ApJ, 764, 167, doi: [10.1088/0004-637X/764/2/167](https://doi.org/10.1088/0004-637X/764/2/167)

Shahbaz, T., Linares, M., & Breton, R. P. 2017, *MNRAS*,

472, 4287, doi: [10.1093/mnras/stx2195](https://doi.org/10.1093/mnras/stx2195)

Shahbaz, T., Linares, M., Rodríguez-Gil, P., & Casares, J.

2019, *MNRAS*, 488, 198, doi: [10.1093/mnras/stz1652](https://doi.org/10.1093/mnras/stz1652)

Stappers, B. W., Archibald, A. M., Hessels, J. W. T., et al.

2014, *ApJ*, 790, 39, doi: [10.1088/0004-637X/790/1/39](https://doi.org/10.1088/0004-637X/790/1/39)

Strader, J., Chomiuk, L., Sonbas, E., et al. 2014, *ApJL*,

788, L27, doi: [10.1088/2041-8205/788/2/L27](https://doi.org/10.1088/2041-8205/788/2/L27)

Strader, J., Chomiuk, L., Cheung, C. C., et al. 2015, *ApJL*,

804, L12, doi: [10.1088/2041-8205/804/1/L12](https://doi.org/10.1088/2041-8205/804/1/L12)

Swihart, S. J., Strader, J., Chomiuk, L., & Shishkovsky, L.

2019, *ApJ*, 876, 8, doi: [10.3847/1538-4357/ab125e](https://doi.org/10.3847/1538-4357/ab125e)

Swihart, S. J., Strader, J., Shishkovsky, L., et al. 2018,

ApJ, 866, 83, doi: [10.3847/1538-4357/aadcab](https://doi.org/10.3847/1538-4357/aadcab)

Szkody, P., Fraser, O., Silvestri, N., et al. 2003, *AJ*, 126,

1499, doi: [10.1086/377346](https://doi.org/10.1086/377346)

Takata, J., Li, K. L., Leung, G. C. K., et al. 2014, *ApJ*,

785, 131, doi: [10.1088/0004-637X/785/2/131](https://doi.org/10.1088/0004-637X/785/2/131)

Tam, P. H. T., Hui, C. Y., Huang, R. H. H., et al. 2010,

ApJL, 724, L207, doi: [10.1088/2041-8205/724/2/L207](https://doi.org/10.1088/2041-8205/724/2/L207)

Thorstensen, J. R., & Armstrong, E. 2005, *AJ*, 130, 759,

doi: [10.1086/431326](https://doi.org/10.1086/431326)

van der Walt, S., Colbert, S. C., & Varoquaux, G. 2011,
Computing in Science Engineering, 13, 22,
doi: [10.1109/MCSE.2011.37](https://doi.org/10.1109/MCSE.2011.37)

van Staden, A. D., & Antoniadis, J. 2016, ApJL, 833, L12,
doi: [10.3847/2041-8213/833/1/L12](https://doi.org/10.3847/2041-8213/833/1/L12)

Virtanen, P., Gommers, R., Burovski, E., et al. 2019,
scipy/scipy: SciPy 1.2.1, v1.2.1, Zenodo,
doi: [10.5281/zenodo.2560881](https://doi.org/10.5281/zenodo.2560881)

Woudt, P. A., Warner, B., & Pretorius, M. L. 2004,
MNRAS, 351, 1015,
doi: [10.1111/j.1365-2966.2004.07843.x](https://doi.org/10.1111/j.1365-2966.2004.07843.x)